Wing Hinge Dynamics Influence Stroke Amplitudes in Flapping Wing Insects: A Frequency Response Approach

Cailin Casey, Braden Cote, Chelsea Heveran, Mark Jankauski

January 20, 2025

Abstract

Flapping insects are thought to leverage resonance or vibration amplification to reduce the energetic costs of flight. However, precisely where resonance occurs within their flight systems remains unclear. We hypothesized that most insects flap near a resonance where elastic deformation occurs primarily within the wing hinge rather than the flexible thorax. To test this, we measured the linear frequency response relating thorax deformation to wing stroke angle in sacrificed honeybees and army cutworm moths. Using experimental data, we developed a linear model of the flight system, which we then extended to incorporate nonlinear effects associated with large wing stroke angles. Our findings revealed that both species flap below the linear resonance of the wing hinge. At large wing stroke angles, nonlinear aerodynamic damping reduces the resonant frequency, causing both species to flap above resonance. However, the wing-hinge resonant frequency varied significantly depending on whether angular position, velocity or acceleration was considered as the frequency response output. Based on these observations, we hypothesized that cutworm moths flap between angular position and velocity resonances, whereas honeybees flap at the angular velocity resonance. The collective results suggest that insects flap in proximity to a wing hinge resonance rather than a thorax resonance.

1 Introduction

The flapping flight of small insects is widely recognized as one of the most energetically demanding forms of locomotion [1]. Unlike many birds, which glide to conserve energy [2], most insects must continuously beat their wings to counteract gravity, resulting in a high metabolic cost. Studies have shown that an insect's metabolic rate during flight can reach levels 50-100 times higher than at rest [3]. To help offset this energetic expense, many insects have evolved a specialized flight mechanism known as indirect actuation, where the insect's indirect flight muscles (IFMs) attach not to the wing base but to the thoracic exoskeleton [4, 5, 6]. When these muscles contract, they cause small deformations in the thorax, which are then amplified into large wing rotations through a complex linkage called the wing hinge [7, 8]. Small steering muscles within the wing hinge adjust its kinematics, allowing for quick, precise maneuvers during flight [9]. Indirect actuation likely helps reduce the energy required for flight by enabling the thorax to store and release energy throughout the wing stroke, functioning as a spring-like structure [10].

Many insects have been assumed to flap their wings at or near the resonant frequency of their flight system to reduce the energetic cost of flight [11, 12, 5]. This is especially true for insects with asynchronous IFMs, which are believed to fire at the resonant frequency of the system to which they are attached rather than the frequency of neurological activation [13]. If an insect flaps at the resonant frequency of its thorax, the force needed by the IFMs to deform the thorax is lower compared to flapping at an off-resonance frequency [14]. Since muscle power depends on both force and strain rate [3], reducing the force required may reduce overall energy consumption. However, if an insect were to deviate their flapping frequency from this resonant frequency, the energetic costs may increase substantially. This poses a trade-off between maneuverability and efficiency, at least if maneuvers are initiated via wingbeat frequency modulation, which has been observed in some Lepidopteran species [12].

Despite the belief that insects flap near resonance, recent studies have challenged this notion. Models of the hawkmoth *Manduca sexta*, for example, suggest that the insect flaps at a higher frequency than its resonant frequency [15]. Flapping post-resonance may enhance the hawkmoth's ability to respond to aerodynamic disturbances by modulating its wingbeat frequency. Further, experimental studies on honeybees have shown that thorax resonant frequency may be higher than their natural flapping frequency, though the artificial boundary conditions and low-amplitude excitation considered in the experiment may cause the measured resonant frequency to be higher than in natural conditions [16]. Others have questioned the simplified concept of resonance in general, proposing that resonance is not a single fixed state but may consist of multiple types within the insect flight system [17]. For instance, the effective resonant frequency differs depending on if wing angular displacement, velocity or acceleration is considered as the kinematic output. Nonetheless, even if insects do not flap exactly at resonance, they may still take advantage of vibration amplification and recycle energy by flapping *near* resonance.

However, if insects do flap near resonance, it is unclear precisely *where* that resonance occurs within the flight system. Simplified models of the insect flight system combine effective stiffness into two spring-like elements: a 'parallel' stiffness element, representing the passive stiffness of the pleural wall in the thoracic exoskeleton, and a torsional 'series' stiffness element, representing the rotational stiffness of the pleural mechanism in the wing hinge [18, 17] (Fig. 1). If the mass of the muscle, exoskeleton and wing are considered, such modeling efforts would predict at least two distinct vibration modes and resonant frequencies. The first is a thorax-dominated mode, which corresponds primarily to deformation of the parallel stiffness element, and the second is a wing hinge dominated mode, which corresponds primarily to deformation of the series stiffness element. We hypothesize that insects operate near or at a wing hinge dominated resonance, where most of the elastic deformation occurs within the wing hinge.

The goals of this work are (1) to identify if wing hinge resonance exists, and if so, (2) to determine the relationship

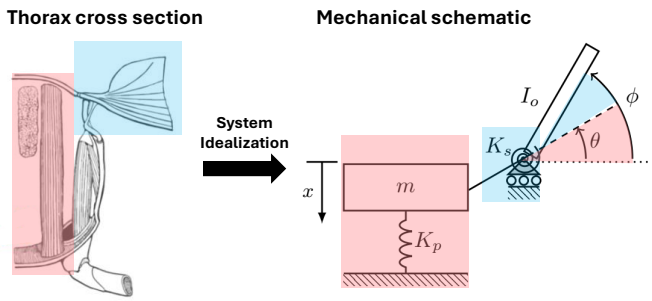

Figure 1: The thorax of insects utilizing indirect actuation (left) can be modeled as a two-degree-of-freedom system (right). In this model, parallel spring with stiffness K_p represents the combined effective stiffness of the thoracic exoskeleton and the passive stiffness of the IFMs, shown in red. A torsional spring with stiffness K_s represents the effective torsional stiffness of the pleural mechanism within the wing hinge, shown in blue. Parameters m and I_o denote the mass of the thorax and IFMs, and the mass moment of inertia of the wing about the wing hinge, respectively. Thoracic deformation, denoted as x, causes the wing to rotate by an angle θ under static conditions. However, under dynamic conditions, the stretching of the series spring modifies the wing's rotation, resulting in an actual rotation angle ϕ. Left image adapted from [19], right image adapted from [18].

between the wing hinge resonant frequency and the insect wingbeat frequency. To this end, we developed a novel experimental approach to measure the frequency response relating thorax deformation to wing stroke angle in sacrificed insects. We considered two insect species: the army cutworm moth *Euxoa auxiliaris*, which is of the Lepidopteran order and has synchronous IFMs, and the honeybee *Apis Mellifera*, which is of the Hymenopteran order and has asynchronous IFMs. We restricted experimental thorax deformation and wing rotation amplitudes such that the flight system was excited primarily within the linear regime. We then utilized a simple mathematical model, populated in part by parameters estimated from the linear experiment, to estimate the nonlinear resonant frequency when the thorax and wings experience large amplitudes.

2 Methods

We developed an experiment to measure the frequency response relating thorax displacement to wing stroke angle in flapping wing insects. The experiment focused on small thorax displacements and wing rotations to evaluate the system's linear response. Using this linear data, we constructed a linear model of the flight system, which was then extended to account for nonlinear aerodynamic effects. The resulting nonlinear model allowed us to estimate how the system's resonant frequency changes with increasing wing stroke angle.

2.1 Specimen care and preparation

We selected the army cutworm moth (*E. auxiliaris*, n = 11) and the honeybee (honeybee, n = 10) as study species. Army cutworm moths and honeybees have synchronous and asynchronous IFMs, respectively. Adult cutworm moths were collected from Powell, WY, and Bozeman, MT, and bred in captivity at Montana State University (Bozeman, MT, USA). Offspring from the F2 generation were used for the experiments. Moths were housed in a 1 m^3 mesh cage at 20°C and fed daily with a 10% sugar solution delivered via soaked cotton balls. Specimens were tested within 10 days after emergence. Honeybees were captured near Montana State University and tested within 90

minutes of capture. All insects were euthanized in an ethyl acetate kill jar. Prior to testing, legs were removed using scissors. Thoracic scales on cutworm moths were gently removed with a damp paper towel.

2.2 Experimental setup and data collection

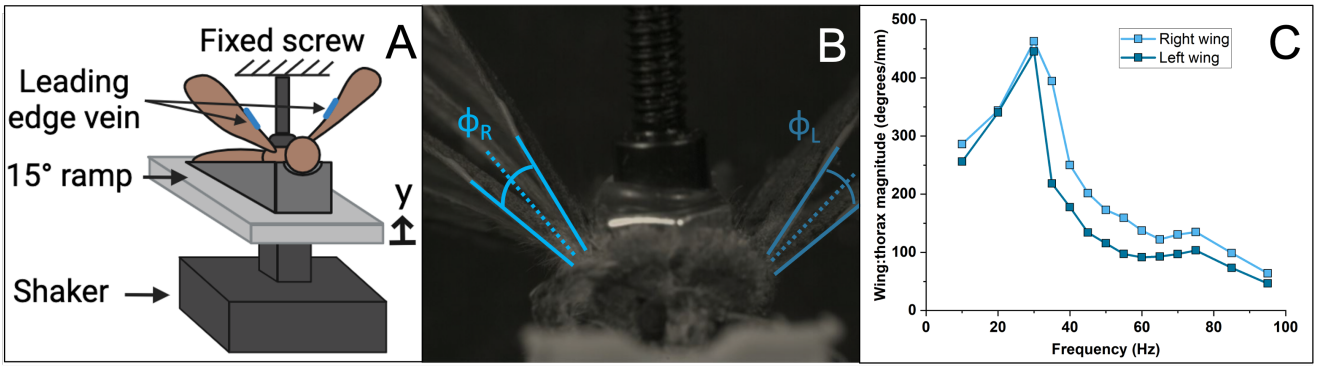

Figure 2: Experimental setup and data analysis. (A) Schematic of the thorax compression setup using a shaker, where y represents the shaker's vertical displacement, assumed to coincide with the displacement of the thorax. (B) Overlaid frames captured by a high-speed camera showing the wing at its maximum upward and downward positions, where ϕ denotes the wing stroke angle amplitude (half the wing stroke). (C) Example frequency response function magnitudes showing the relationship between wing stroke angle and thorax displacement for the left and right wings.

The experimental setup used to measure the frequency response between thorax deformation and wing stroke angle is shown in Fig. 2A. Thorax deformation was induced in sacrificed insects using an electrodynamic vibration shaker (2007E, The Modal Shop, Cincinnati, OH, USA), which caused the wings to rotate. For cutworm moth, the ventral thorax was adhered to a 3D-printed 15° ramp with cyanoacrylate to approximate the natural body pitch angle during flight [20]. The dorsal thorax was secured with glue to a #2 hex nut (approximately 4.8 mm in diameter). For honeybees, the ventral thorax was glued in a similar manner, but without an incline, to align with the dorso-ventral flight muscles [21]. The dorsal thorax was attached to a #2 set screw (approximately 2.2 mm in diameter). For all specimens, the screw was positioned to ensure consistent thorax compression throughout the displacement range, with no repositioning required during testing. To aid in tracking, a dot of nail polish was applied to the leading-edge vein (Fig. 2A). After setup, the insects remained in a compressed position for 10 minutes to allow the glue and nail polish to dry fully.

The thorax was displaced harmonically via an electrodynamic shaker (2007E, The Modal Shop, Cincinnati, OH, USA). The input voltage to the shaker was modulated via a signal generator (SDG 1032X, Siglent, Solon, OH USA). A high-speed camera (Chronos 2.1, Kron Technologies, Burnaby, BC Canada) with macro lens (100mm f/2.8, Rokinon, New York, NY USA) was used to capture the wing rotation during testing. Frame rates of 2142 frames per second and 7135 frames per second were used for cutworm moth and honeybees, respectively. The camera was set level with the insect to capture the projection of the wing stroke angle onto the insect's transverse plane (Fig. 2B). We refer to this angle as the wing stroke angle hereafter. Insects were tested in a frequency range that encompassed their known flapping frequencies. Cutworm moth specimens were compressed at 14 discrete frequencies between 10 and 95 Hz (*in vivo* flapping frequency of 41 ± 4.3 Hz [22]). Honeybee specimens were tested at 13 discrete

frequencies between 50 and 350 Hz (*in vivo* flapping frequency of 230 Hz ± 8.8[23]).

Shaker displacement, assumed to coincide with thorax deformation at the location of the fixed screw, was also measured. For cutworm moths, an identical high speed camera with a 35mm lens (Rokinon, New York, NY USA) was synchronized with the first and positioned level with the shaker stage to measure vertical displacement. While similarly sized moths (*Helicoverpa Zea* and *Agrotis ipsilon*) had *in vivo* thorax displacements of 0.214 and 0.290 mm during tethered flight [24], we imposed smaller thorax compression amplitudes during this experiment ($35 \pm 3.2\mu$m) to minimize the potential influence of nonlinearities (e.g., quadratic aerodynamic damping acting on the wing) on the frequency response. During testing, the shaker was started about a second before video recording commenced, so that only steady-state behavior was captured. Only the first wing cycle was analyzed for each frequency. The same procedure was followed for honeybees. A compression amplitude of $4.8 \pm 0.35\mu$m was imposed on the thorax, which is lower than the thorax deformation amplitudes ($\sim 50\mu$m) observed during tethered flight of the similarly sized bumblebees [25]. For honeybees, such small shaker displacements could not be accurately observed using our high-speed videography equipment. We instead used a laser vibrometer (VibroGo VGO-200, Polytec, Baden-Württemberg,Germany) trained on the shaker stage supporting the insect to measure thorax displacement. Euthanasia to completion of testing took between 40 and 60 minutes for each insect. The exact measured shaker displacements for all subjects across all frequencies are shown in Fig. S1.

2.3 Data analysis

Wing position was tracked using DLTdv8 point software [26]. Four points were tracked for each specimen: one point at each root and one point each along the leading edge vein of the left and right wings. Wing stroke angle was calculated from the tracked points (Fig. 2C). The points on the leading edges were chosen in the first 50% of the wing length to minimize the potential confounding influence of wing deformation on rigid body wing stroke angle.

This study aimed to measure the wing stroke angle; however, wing pitching may have introduced some error into this measurement. The wing's pitching rotation does not perfectly align with the leading-edge vein, as the pitching axis lies between the leading edge and the mid-chord line in hawkmoths [27] and perhaps in other insects as well. Consequently, pitch rotations could affect the calculated wing stroke angle. Despite this, we believe the error is small. High-speed video observations reveal relatively pitching at the small thorax displacements used in the experiment (though pitching tended to increase at the highest frequencies tested in honeybees; see supplementary material). Further, we tracked points along the leading edge vein near the wing root, where the the pitching axis and leading edge vein are nearly coincident in some insects [28]. Multiple high-speed cameras would be required to capture the wing's three-dimensional kinematics and fully decouple the wing's stroke and pitch rotations, which was beyond the scope of the present work.

A Savitzky-Golay filter was applied to all time series data collected from the camera – both the left and right wing strokes, and the thorax displacement for cutworm moths. For cutworm moths, the filter had a frame size of 21 data points and an order of 3, meaning that every 21 points were fitted to a third degree polynomial. For honeybees, the frame size was smaller, 15 points, because there were very few data points per curve at the highest frequencies. The magnitude frequency response function relating the input of thorax compression to the output of wing stroke was calculated by normalizing the mean wing stroke amplitude by the mean thorax compression amplitude at each frequency (Fig. 2C).

2.4 Frequency response curve fitting

Once the linear frequency response was determined experimentally, we fit a linear single-degree-of-freedom dynamical model relating thorax displacement x and stroke angle ϕ. The model is parameterized by natural frequency (ω_n), damping ratio (ζ), and gain coefficient (A). The natural frequency and the damping ratio were estimated for each wing individually by least square curve fitting the magnitude data to a curve according to the following equation:

$$\left|\frac{\phi}{x}\right| = \frac{A}{\sqrt{(\omega^2 - \omega_n^2)^2 + (2\omega\omega_n\zeta)^2}} \tag{1}$$

For cutworm moths, A was bounded between 0 and $1 \times 10^9 \frac{\text{rad}\cdot\text{s}^2}{\text{m}}$, ζ between 0 and 2, and ω_n between 0 and $100 \times 2\ \pi\ \frac{\text{rad}\cdot\text{s}^2}{\text{m}}$. For honeybees, A was bounded between 0 and $1 \times 10^{11} \frac{\text{rad}}{\text{m}}$, ζ between 0 and 2, and ω_n between 0 and $5000 \times 2\pi\ \frac{\text{rad}}{\text{s}}$. We used a least squares procedure to curve fit the function with a tolerance of 1×10^{-12} and an optimality tolerance of 1×10^{-12} (MATLAB version R2024b). For both species, the frequency response magnitude data for the lowest and two highest experimental frequencies were excluded before performing curve fitting. This helped to reduce the influence of higher-order resonances on the accuracy of curve fitting around the wing hinge dominated resonance. We then discarded fits that had an r^2 value less than 0.8, which reduced our effective sample size to $n = 19$ army cutworm wings and $n = 17$ honeybee wings (i.e., data from 3 wings discarded from each species). Poor fits generally occurred when there was no identifiable peak within the frequency range tested.

2.5 Modeling

The experiment carried out in this work is designed to operate within the linear regime of the insect flight system. However, aerodynamic damping acting on the wing at large stroke amplitudes introduces a quadratic nonlinearity – hence, we expect the shape and resonance of the frequency response to be affected by the amplitude of the input thorax deformation [15]. We developed a mathematical model to estimate how the frequency response relating thorax displacement to wing stroke angle changes at large input thorax deformation amplitudes (Fig. 3).

Suppose that the thorax deformation is x, which is prescribed within the experiment and consequently can be neglected as an independent degree-of-freedom. The thorax connects to the base of the wing via a rigid lever. Thorax deformation x is algebraically related to the angle prescribed at the base of the wing θ by $\theta = \frac{x}{\gamma}$, where γ is the wing-thorax transmission ratio. Due to local compliance, the wing is permitted to rotate beyond what is prescribed at the wing base by the thorax deformation. Actual wing rotation is defined as ϕ. The aerodynamic moment acting on the wing is determined through a blade element approach [29, 30]. We use a moment balance about the wing base to derive the equation of motion governing ϕ as

$$I_O\ddot{\phi} + C_S\left(\dot{\phi} - \frac{\dot{x}}{\gamma}\right) + K_S\left(\phi - \frac{x}{\gamma}\right) + \frac{1}{8}\rho_f C_D b L^4 \dot{\phi}|\dot{\phi}| = 0 \tag{2}$$

where K_s and C_s are the torsional stiffness and damping at the wing base, respectively, I_o is the wing's mass moment of inertia about its base, ρ_f is fluid density, b is the wing's chord width (assumed constant), L is the wing length and C_D is a drag coefficient.

The model parameters were populated using a combination of anatomical measurements, literature, and experimental data (Tab. 2). We modeled the wing as a thin, uniform, rigid rectangle. The wing's mass moment of inertia is $I_o = \frac{1}{3}mL^2$, where m is the wing's mass. The forewings were massed (AS 60/220.R2 Plus, Radwag, Radom Poland) and their length and maximum width were measured using ImageJ [31]. All wing measurements were averaged

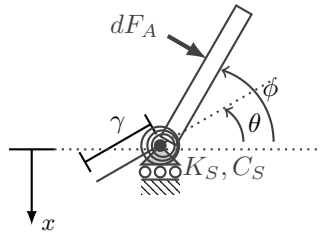

Figure 3: Simple mechanical model of the insect flight system. x denotes thorax deformation, which algebraically relates to the angle θ prescribed at the base of the wing by $\theta = \frac{x}{\gamma}$, where γ is the transmission ratio. The actual wing angle is denoted ϕ. The effective torsional stiffness and damping at the wing hinge are K_s and C_s, respectively. dF_a is a differential aerodynamic force acting on the wing, which is integrated over the wing surface to yield the total aerodynamic force and moment.

from the left and right wings of two individuals and are for the forewings only. Air density was based on its density at standard temperature and pressure. We considered drag coefficients of 2, which is based on the drag coefficient range reported in [32]. While the drag coefficient varies temporally with angle of attack in real flapping wings, our models assume that the wing experiences only single degree-of-freedom rotation and consequently has a constant angle of attack; the drag coefficient is thus treated as a constant. The remaining model parameters were populated using fitted frequency response data. The torsional stiffness and damping at the wing base are calculated based on the system's fitted natural frequency and damping ratio (Eq. 1) and the wing's idealized moment of inertia. The transmission ratio is inferred from the static gain of the frequency response.

Thorax displacement, including displacement amplitude and frequency, served as the model input. Thorax displacement was assumed harmonic and its amplitude was varied in both insects such that the resulting wing stroke amplitudes spanned from the experimental range to the *in vivo* range. This yielded displacement amplitudes of 35, 100, 250 and 500 μm for cutworm moth and 5, 25, 75, 150 μm for honeybees. The model was used to find the steady-state wing stroke amplitude over a frequency range similar to the experimental range (1 to 100 Hz for cutworm moth and 1 to 350 Hz for honeybees). For each frequency, the model was solved at 1000 time points over 20 wingbeats to reach steady state using ODE45 (MATLAB version R2024b). The stroke amplitude of the final wingbeat was used to calculate the ratio of wing stroke amplitude to thorax displacement amplitude.

3 Results

3.1 Experimental results

The frequency response magnitudes for each insect, separated by left and right wings, are shown in Fig. 4A,B,D,E. Individual magnitude curves were fitted via Eq. 1 to identify the gain coefficient, natural frequency, and damping ratio for each insect. Each quantity was subsequently averaged to obtain the data shown in Tab. 1. We then used the average data from Tab. 1 to calculate a frequency response magnitude representative of all subjects within a species, shown in Fig. 4C,F. According to the representative frequency response magnitude plots, the resonant frequency is about 52.7 Hz in army cutworms and 219.7 Hz in honeybees. This is lower than the system natural frequencies reported in Tab. 1, which is expected in systems with modest damping. Both insects displayed relatively low damping ratios. Representative videos of the wing stroke angle at pre, near and post resonance conditions for

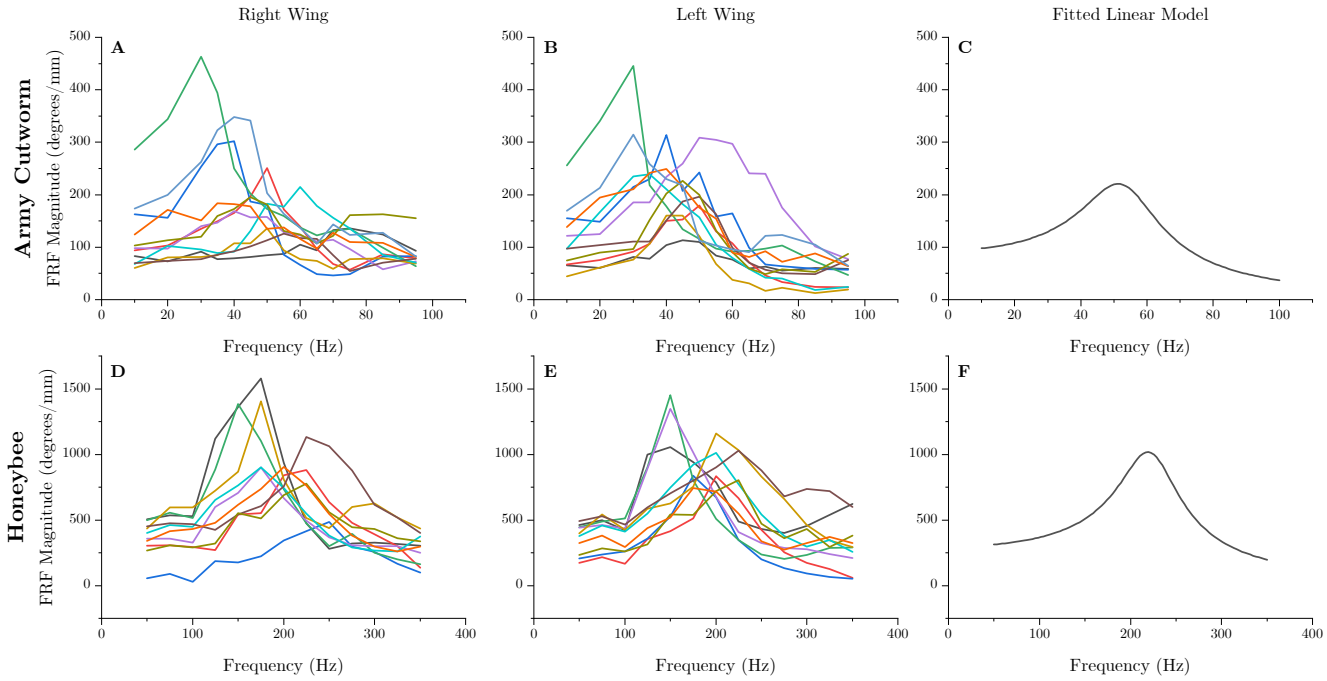

Figure 4: Frequency response magnitude as a function of excitation frequency for all subjects. The right-hand panels plot Eq. 1 populated with the average natural frequencies, damping ratios and gain factors reported in Tab. 1, which represents a typical frequency response magnitude for each species.

both species are shown in supplementary material.

3.2 Modeling results

The parameters used in the numerical models are listed in Tab. 2. Figure 5 illustrates the frequency response amplitude and response stroke angle amplitude for varying levels of thorax compression in both species. For the army cutworm, at low thorax deformation amplitudes, the flapping frequency is lower than the flight system's resonant frequency. However, as the thorax deformation amplitude increases, the flapping frequency surpasses the resonant frequency. In the case of the honeybee, the flapping frequency matches the flight system's resonant frequency at small thorax deformation amplitudes. With greater thorax deformation, the flapping frequency exceeds the resonant frequency. In both species, the observed reduction in resonant frequency at high thorax deformation amplitudes is caused by nonlinear aerodynamic damping. Real flapping wing insects exhibit stroke amplitudes of approximately 45 - 60° [23, 20], which the model predicts occurs only near the highest amplitudes of thorax deformation considered.

4 Discussion

It has long been presumed that most insects flap at or near the resonant frequency of their flight system to reduce the energetic costs of flapping wing flight. However, it is unclear precisely where this resonance occurs within the

Table 1: Linear frequency response parameters. Wing responses were averaged across all individuals (mean ± standard deviation). Left and right wings are treated as individual trials.

Description	Variable	Army Cutworm	Honeybee	Units
Sample size	n	19	17	-
Gain Coefficient	A	$(1.91 \pm 0.66) \times 10^2$	$(1.03 \pm 0.42) \times 10^4$	$\frac{\text{rad}\cdot\text{s}^2}{\mu\text{m}}$
Natural Frequency	ω_n	53.98 ± 9.78	224.14 ± 30.33	Hz
Damping Ratio	ζ	0.22 ± 0.06	0.15 ± 0.04	-

flight system. Recent studies have considered the flight system to have two sources of stiffness: a parallel spring, representative of the stiffness of the indirect flight muscles and exoskeleton, and a series spring, representative of the torsional stiffness of the wing hinge [18]. Based on these ideas, we hypothesized that the flight system has a resonant frequency that corresponds primarily to stretching of the wing hinge. We refer to this as a wing hinge resonant frequency hereafter.

To determine if wing hinge resonance plays a role in the dynamics of the insect flight system, we experimentally measured the frequency response relating thorax deformation to wing stroke angle in two insect species: the army cutworm, which has synchronous indirect flight muscles, and the honeybee, which has asynchronous indirect flight muscles. At small thorax deformations, we assumed that the flight system could be treated as a single degree-of-freedom oscillator. We fit the oscillator parameters, specifically natural frequency, damping ratio and gain factor, based on experimental data. We subsequently extended the linear model to incorporate the nonlinear aerodynamic damping associated with large thorax deformations and stroke angles, and used this nonlinear model to identify if nonlinear resonant frequencies deviated from linear resonant frequencies. In this section, we contextualize our findings within the broader field of insect flight.

4.1 Do insects flap at a wing hinge resonance?

Our collective findings suggest that both the army cutworm and the honeybee have a wing hinge resonance in proximity to their flapping frequency. Specifically, the army cutworm flaps at approximately 41 Hz [22] and the

Table 2: Model parameters.

Symbol	Equation	Army Cutworm	Honeybee	Units
ζ		0.26	0.17	-
ω_n		50	204	Hz
L		19	8.1	mm
b		7.0	2.3	mm
m		1.9	0.15	mg
ρ_f		1.25	1.25	$\frac{\text{kg}}{\text{m}^3}$
C_D		2	2	-
I_O	$\frac{1}{3}mL^2$	2.28×10^{-10}	3.28×10^{-12}	$\text{kg} \cdot \text{m}^2$
K_S	$\omega_n^2 I_O$	2.63×10^{-5}	6.51×10^{-6}	$\frac{\text{N}\cdot\text{m}}{\text{rad}}$
C_S	$2\zeta\omega_n I_O$	3.41×10^{-8}	1.39×10^{-9}	$\frac{\text{N}\cdot\text{m}\cdot\text{s}}{\text{rad}}$
γ	$\frac{\omega_n^2}{A}$	6.14×10^{-4}	1.92×10^{-4}	$\frac{\text{m}}{\text{rad}}$

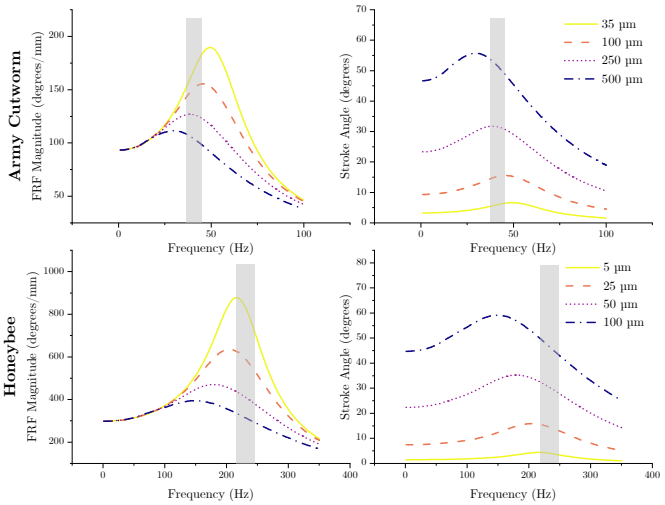

Figure 5: Nonlinear modeling predictions of the frequency response magnitude and wing stroke angle as a function of flapping frequency for both species and various thorax deformation amplitudes. The gray regions indicate the reported flapping frequency range for both species.

honeybee at about 230 Hz [23], while small amplitude experiments identified linear resonant frequencies of roughly 53 Hz and 220 Hz respectively (Fig. 4). This implies that both species flap below their linear resonant frequencies. However, as wing stroke amplitudes increase to *in vivo* values, mathematical models predict that both species flap at frequencies above nonlinear resonance (Fig. 5). These results align with mathematical modeling for the hawkmoth *M. sexta* [15]. Nevertheless, additional factors must be considered before definitively concluding that both species function within a post-resonant regime.

First, multiple types of resonance may exist within the flight system [17]. In our experiment, we measured the frequency response between thorax deformation to wing stroke angle, which are both position variables. However, the resonant frequency will be different depending on if angular position, velocity or acceleration is considered as the kinematic output. A displacement-displacement frequency response typically has a resonant frequency lower than the system's natural frequency when damping is present [33]. By contrast, a displacement-velocity frequency response has a resonant frequency nearly equivalent to the system's natural frequency and a displacement-acceleration higher than the system's natural frequency [33]. To explore these alternative resonant states, we plot the response angle, angular velocity and angular acceleration determined via the nonlinear model for various thorax deformation amplitudes in Fig. 6. At the largest thorax deformation amplitudes considered, the flapping frequency of the army cutworm falls between the angular displacement and angular velocity resonant frequencies. For the honeybee, the flapping frequency is nearly coincident with the angular velocity resonance. It is possible that differing species, particularly those with different types of IFMs, leverage different types of resonance to realize flight. We hypothesize that insects with synchronous IFMs operate off position and velocity based resonances, which would underpin their ability to respond to environmental perturbations such as wind gusts via wingbeat frequency modulation. We further hypothesize that insects with asynchronous IFMs operate near or at a velocity resonance, and are more reliant on kinematic adjustments made through the wing hinge to respond to flight disturbances.

Second, muscle dynamics may influence the system's effective resonant frequency, particularly in the case of the

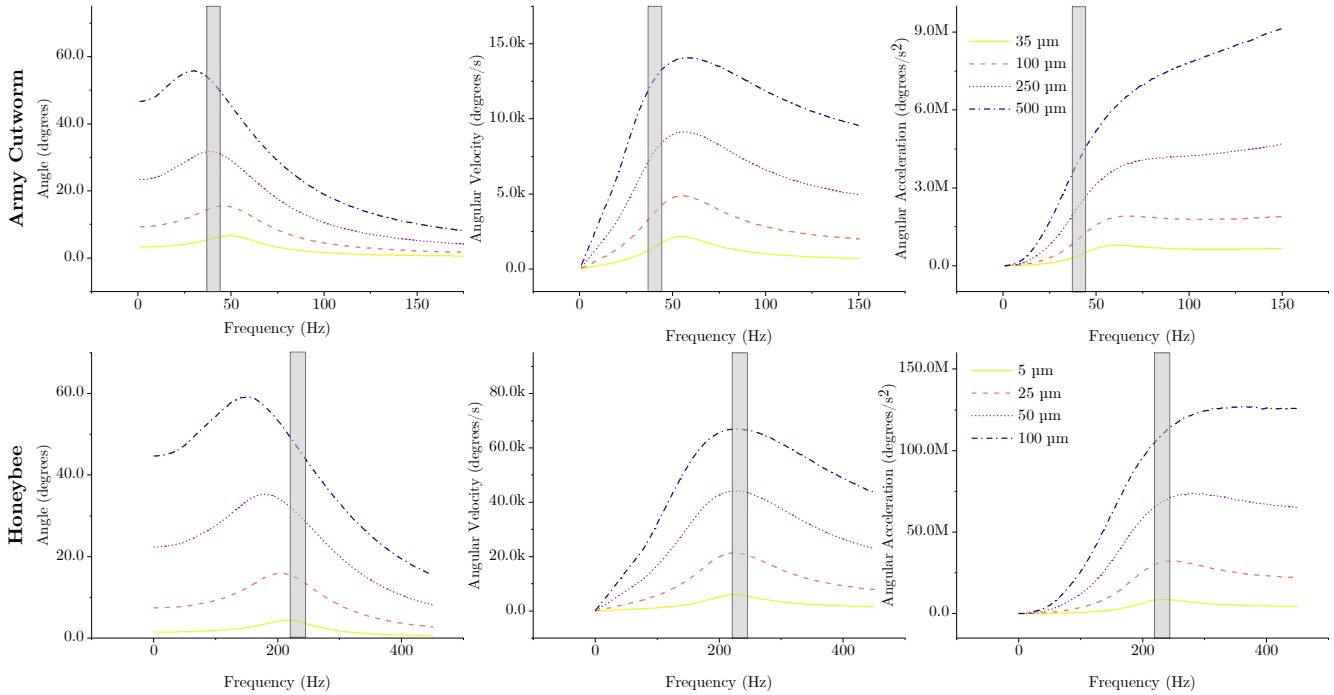

Figure 6: Mathematical model predictions of angular displacement, velocity and acceleration responses for various thorax deformation amplitudes. The gray box indicates the approximate flapping range for both species.

honeybee with asynchronous IFMs. Asynchronous muscle models suggest that the force they produce is proportional to the muscle strain rate processed through a second-order low-pass filter [34]. Because muscle forces are a function of muscle strain rate and not simply time, they must be considered among the flight system's dynamical state and consequently influence the system's resonant frequencies. All experiments in this work considered sacrificed insects with inactive IFMs; the present experiment captures only the *mechanical* resonance of the wing hinge. Inclusion of muscle dynamics may lead to a *musculo-mechanical* resonance, which may occur at a frequency different than the mechanical resonance depending on the specific muscle properties. Although we expect the muscle dynamics influence the resonant frequency more in insects with asynchronous IFMs, it is possible that muscle dynamics influence resonant frequencies in insects with synchronous IFMs as well. Recent evidence in the hawkmoth *M. sexta* show that their synchronous flight muscles exhibit delayed stretch activation, a property usually attributed to asynchronous muscles [35]. Consequently, the possibility of musculo-mechanical resonance should not be ignored in insects with synchronous IFMs.

Finally, wing-wing coupling through the flexible thorax may affect flight system resonant frequencies. Experimentally, we prescribed thorax deformation rather than the forces acting on the thorax. This restricts backward coupling between the wing and the thorax (that is, the thorax motion influences the wing, but wing dynamics cannot influence the deformation of the thorax at the parallel spring location) as well as wing-wing coupling through the thorax. The wings can therefore behave as independent oscillators, which is why the left and right wings of an individual insect may have different resonant frequencies (Fig. 4). Experimentally, the left-right resonant frequencies may

differ if the set screw actuating the thorax is slightly misaligned, or if there is difference in initial wing orientation when the insect is sacrificed. Previous studies in flies support the idea that the wings can behave as independent oscillators, where disruption of thorax-mediated wing-wing coupling led to disparate flapping frequencies between wing pairs [11]. Should the thorax flexibility be taken into account, we expect that the flight system will be moderately more flexible as a whole, thus lowering all resonant frequencies. It is also possible that wing flexibility, which is neglected in the present model, affects the flight system resonant frequency; several studies have highlighted the importance of wing flexibility to energetics and system dynamics [36, 37, 38].

4.2 Parallel and Series Stiffness

In a previous study, we hypothesized that wing hinge stretching (i.e., stretching of the flight system series spring element) played a more pronounced role in the flight of insects with asynchronous IFMs compared to those with synchronous IFMs [24]. This was based on the idea that wing-generated inertial forces were determined to be larger in insects with asynchronous IFMs due to an increased wing surface density [39]. We hypothesized that the increased inertial forces resulting from the large surface density would cause the wing hinge to stretch more during flapping. However, this assertion relied on the assumption that the wing hinge was similarly stiff (when accounting for scaling effects) in insects of both IFM types. Here, we expand upon this hypothesis equipped with a quantitative estimate of wing hinge stiffness.

It can be shown that the series to parallel stiffness ratio $\mathcal{S} = \frac{K_p \gamma^2}{K_s}$, where K_p is the parallel stiffness, K_s is the series stiffness, and γ is the transmission ratio. The latter two quantities are reported in Tab. 2. We did not calculate K_p in the present study for the honeybee or army cutworm moth. We instead estimated K_p for the honeybee using values for *Bombus centralis* ($K_P = 973$ N/m) and for the army cutworm using values for *Agrotis ipsilon* ($K_P = 481$ N/m) because they are of similar size and have the same muscle type as the test species [24]. Using these values, we arrive at stiffness ratios of $\mathcal{S} = 6.9$ for the army cutworm and $\mathcal{S} = 5.5$ for the honeybee. Thus, the relative stiffness of the series spring appears to similar in the honeybee compared to the army cutworm – and for both species, the relative stiffness of the parallel spring is higher than that of the series spring.

Given the similar wing hinge stiffness between the species, and the higher wing surface density in the honeybee, it is likely that wing hinge stretching is greater in the honeybee compared to the army cutworm moth. To highlight this point, we plotted the wing hinge stretch predicted by the nonlinear model under different thorax deformation amplitudes (defined mathematically as $\max(|\phi - \theta|)$) in Fig. 7. Despite operating closer to a angular position resonance, the army cutworm has lower wing hinge stretching compared to the honeybee across all thorax deformation amplitudes considered within the naturally observed flapping frequency range. Thus, absent contributions from steering muscles within the wing hinge, we hypothesize that wing hinge stretching plays a more considerable role in insects with asynchronous IFMs compared to those with synchronous IFMs. Additional efforts must be made to better understand how moments imparted by the steering muscle influences wing hinge dynamics.

Moreover, due to the stiffness ratios calculated for both insects, we hypothesize that the wing hinge resonance occurs at a frequency lower than a thorax resonant in both species. A stiffness ratio greater than one implies that the relative stiffness of the parallel spring is higher than that of the series spring. The wing hinge resonance is governed primarily by the stiffness of the series spring and wing inertia, whereas a thorax resonance is governed by the stiffness of the parallel spring and the effective mass of the IFMs and exoskeleton. Given the higher stiffness of the parallel spring and an assumption that the effective mass of the IFMs and exoskeleton is lower than that of wing inertia (when converting between angular and translational coordinates), the thorax resonant frequency is likely much higher than that of the wing hinge. Therefore, in flapping wing insects, we expect that resonance (or

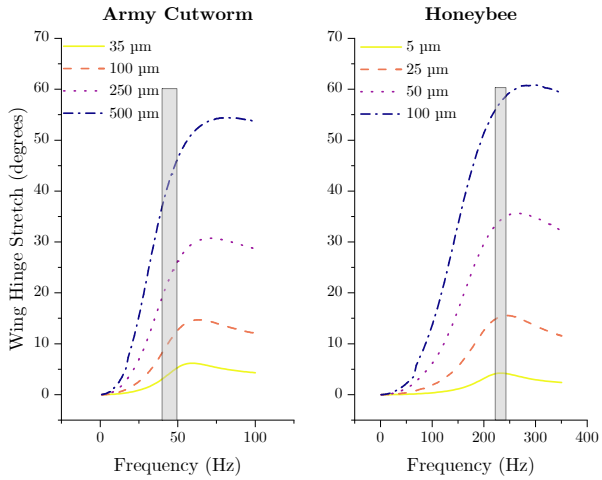

Figure 7: Mathematical model predictions of wing hinge stretch amplitude, defined as $\max(|\phi - \theta|)$, for various thorax deformation amplitudes. The gray box indicates the approximate flapping frequency range for both species.

near resonance) occurs primarily within the wing hinge rather than the thorax, regardless of the resonance type.

Funding

This research was supported by the National Science Foundation under award no. 2043105 to C.C and CMMI-1942810 to MJ. Any opinions, findings, and conclusions or recommendations expressed in this material are those of the author(s) and do not necessarily reflect the views of the National Science Foundation.

Acknowledgments

We would like to thank Taylor Kennedy for raising the *E. auxiliaris* specimens.

Data Availability

The data and models supporting this work are available at https://zenodo.org/records/14675752.

Supplemental

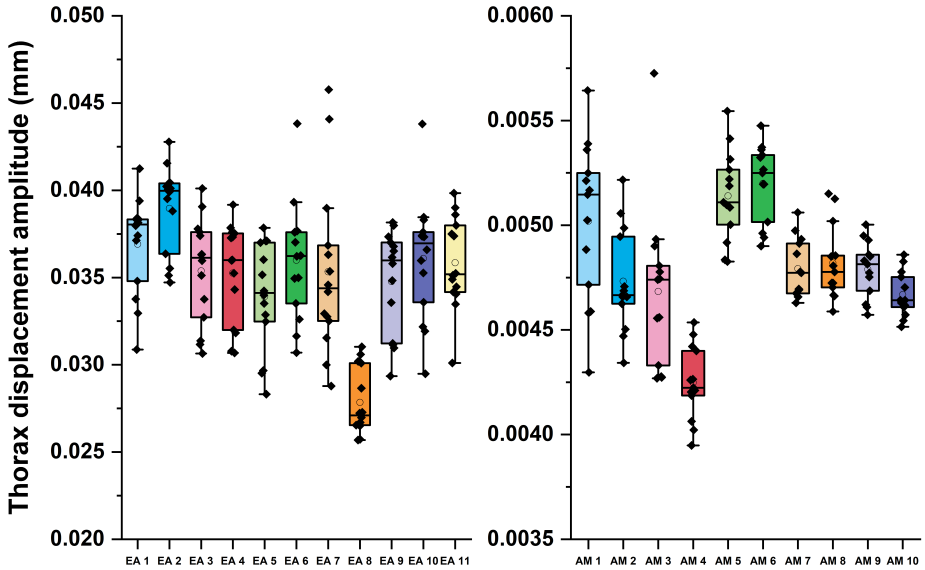

Figure S1: Boxplots for the displacement amplitudes for each specimen. Left plots are for the army cutworm, and right plots are for the honeybee.

References

[1] R McNeill Alexander. Models and the scaling of energy costs for locomotion. *Journal of Experimental Biology*, 208(9):1645–1652, 2005.

[2] Bret W Tobalske. Air sacs reduce energy costs for soaring birds, 2024.

[3] Charles P Ellington. Power and efficiency of insect flight muscle. *Journal of Experimental Biology*, 115(1):293–304, 1985.

[4] Mark Jankauski, Cailin Casey, Chelsea Heveran, M Kathryn Busby, and Stephen Buchmann. Carpenter bee thorax vibration and force generation inform pollen release mechanisms during floral buzzing. *Scientific Reports*, 12(1):12654, 2022.

[5] J. W. S. Pringle. The excitation and contraction of the flight muscles of insects. *The Journal of Physiology*, 108, 3 1949.

[6] Hiroyuki Iwamoto. Structure, function and evolution of insect flight muscle. *Biophysics*, 7:21–28, 2011.

[7] W Nachtigall, A Wisser, and D Eisinger. Flight of the honey bee. viii. functional elements and mechanics of the "flight motor" and the wing joint–one of the most complicated gear-mechanisms in the animal kingdom. *Journal of comparative Physiology B*, 168:323–344, 1998.

[8] Mary B Rheuben and A E Kammer. Structure and innervation of the third axillary muscle of manduca relative to its role in turning flight. *Journal of Experimental Biology*, 131:373–402, 1987.

[9] Anders Hedenström. How insect flight steering muscles work. *PLoS biology*, 12(3):e1001822, 2014.

[10] Jeff Gau, Nick Gravish, and Simon Sponberg. Indirect actuation reduces flight power requirements in manduca sexta via elastic energy exchange. *Journal of the Royal Society Interface*, 16, 12 2019.

[11] Tanvi Deora, Namrata Gundiah, and Sanjay P Sane. Mechanics of the thorax in flies. *Journal of Experimental Biology*, 220(8):1382–1395, 2017.

[12] Jeff Gau, Ryan Gemilere, LDS-VIP (FM subteam), James Lynch, Nick Gravish, and Simon Sponberg. Rapid frequency modulation in a resonant system: aerial perturbation recovery in hawkmoths. *Proceedings of the Royal Society B*, 288(1951):20210352, 2021.

[13] Robert K Josephson, Jean G Malamud, and Darrell R Stokes. Asynchronous muscle: a primer. *Journal of Experimental Biology*, 203(18):2713–2722, 2000.

[14] Braden Cote, Samuel Weston, and Mark Jankauski. Modeling and analysis of a simple flexible wing—thorax system in flapping-wing insects. *Biomimetics*, 7(4):207, 2022.

[15] Jeff Gau, Ethan S Wold, James Lynch, Nick Gravish, and Simon Sponberg. The hawkmoth wingbeat is not at resonance. *Biology Letters*, 18:20220063, 2022.

[16] Mark A Jankauski. Measuring the frequency response of the honeybee thorax. *Bioinspiration and Biomimetics*, 15, 2020.

[17] Arion Pons and Tsevi Beatus. Distinct forms of resonant optimality within insect indirect flight motors. *Journal of The Royal Society Interface*, 19:20220080, 6 2022. doi: 10.1098/rsif.2022.0080.

[18] James Lynch, Jeff Gau, Simon Sponberg, and Nick Gravish. Dimensional analysis of spring-wing systems reveals performance metrics for resonant flapping-wing flight. *Journal of the Royal Society Interface*, 18:20200888, 2021.

[19] Robert E Snodgrass. *Principles of insect morphology*. Cornell University Press, 2018.

[20] Alexander P Willmott and Charles P Ellington. The mechanics of flight in the hawkmoth manduca sexta. i. kinematics of hovering and forward flight. *The Journal of experimental biology*, 200:2705–2722, 1997.

[21] Robert E Snodgrass. *The thorax of the Hymenoptera*, volume 39. US Government Printing Office, 1910.

[22] Clare Mikaela Dittemore. Natal origin, migratory patterns, and abundance of the army cutworm moth, euxoa auxiliaris. 2022.

[23] Douglas L Altshuler, William B Dickson, Jason T Vance, Stephen P Roberts, and Michael H Dickinson. Short-amplitude high-frequency wing strokes determine the aerodynamics of honeybee flight. *Proceedings of the National Academy of Sciences*, 102:18213–18218, 2005.

[24] Cailin Casey, Chelsea Heveran, and Mark Jankauski. Experimental studies suggest differences in the distribution of thorax elasticity between insects with synchronous and asynchronous musculature. *Journal of the Royal Society Interface*, 20:20230029, 2023.

[25] Braden Cote, Cailin Casey, and Mark Jankauski. Wing inertia influences the phase and amplitude relationships between thorax deformation and flapping angle in bumblebees. *Bioinspiration & Biomimetics*, 2024.

[26] Tyson L Hedrick. Software techniques for two-and three-dimensional kinematic measurements of biological and biomimetic systems. *Bioinspiration & biomimetics*, 3:034001, 2008.

[27] Qi Wang, J F L Goosen, and Fred van Keulen. Optimal pitching axis location of flapping wings for efficient hovering flight. *Bioinspiration & biomimetics*, 12:056001, 2017.

[28] Thomas Engels, Dmitry Kolomenskiy, Kai Schneider, Marie Farge, Fritz-Olaf Lehmann, and Jörn Sesterhenn. Helical vortices generated by flapping wings of bumblebees. *Fluid Dynamics Research*, 50:011419, 2018.

[29] Mark Jankauski, Tom Lewis Daniel, and IY Shen. Asymmetries in wing inertial and aerodynamic torques contribute to steering in flying insects. *Bioinspiration & biomimetics*, 12(4):046001, 2017.

[30] Michael H Dickinson, Fritz-Olaf Lehmann, and Sanjay P Sane. Wing rotation and the aerodynamic basis of insect flight. *science*, 284(5422):1954–1960, 1999.

[31] Caroline A Schneider, Wayne S Rasband, and Kevin W Eliceiri. Nih image to imagej: 25 years of image analysis. *Nature methods*, 9:671–675, 2012.

[32] John P Whitney and Robert J Wood. Aeromechanics of passive rotation in flapping flight. *Journal of fluid mechanics*, 660:197–220, 2010.

[33] Leonard Meirovitch. *Fundamentals of vibrations*. Waveland Press, 2010.

[34] James Lynch, Jeff Gau, Simon Sponberg, and Nick Gravish. Autonomous actuation of flapping wing robots inspired by asynchronous insect muscle. In *2022 International Conference on Robotics and Automation (ICRA)*, pages 2076–2083. IEEE, 2022.

[35] Jeff Gau, James Lynch, Brett Aiello, Ethan Wold, Nick Gravish, and Simon Sponberg. Bridging two insect flight modes in evolution, physiology and robophysics. *Nature*, 622(7984):767–774, 2023.

[36] Ryan Schwab, Joseph Reade, and Mark Jankauski. Quasi three-dimensional deformable blade element and unsteady vortex lattice reduced-order modeling of fluid–structure interaction in flapping wings. *Physics of Fluids*, 34(12), 2022.

[37] Heidi E Reid, Ryan K Schwab, Miles Maxcer, Robert KD Peterson, Erick L Johnson, and Mark Jankauski. Wing flexibility reduces the energetic requirements of insect flight. *Bioinspiration & biomimetics*, 14(5):056007, 2019.

[38] Joseph Reade and Mark Jankauski. Investigation of chordwise functionally graded flexural rigidity in flapping wings using a two-dimensional pitch–plunge model. *Bioinspiration & Biomimetics*, 17(6):066007, 2022.

[39] Ngoc San Ha, Quang Tri Truong, Nam Seo Goo, and Hoon Cheol Park. Relationship between wingbeat frequency and resonant frequency of the wing in insects. *Bioinspiration biomimetics*, 8:046008, 2013.